Chronic Extreme Humid Heat as an Emerging Climatic Constraint on Human Activity

Tiffanie Lescure & Dimitri Defrance

Affiliation: CosmosClimae, Montpellier, France
Email: dimitri@cosmosclimae.com

Preprint Statement

This manuscript is a non-peer reviewed preprint submitted to EarthArXiv. It has also been submitted for peer review to Theoretical and Applied Climatology. The content of this preprint has not yet undergone formal peer review. Subsequent versions of this manuscript may differ from this version.

Date: 03/03/2026March 3, 2026

Future heat-stress regimes under CMIP6: a multi-index assessment of persistence and human-relevant thermal constraints

Tiffanie Lescure[1] and Dimitri Defrance[1*]

[1]CosmosClimae, Montpellier, 34000, Occitanie, France.

*Corresponding author(s). E-mail(s): dimitri@cosmosclimae.com;
Contributing authors: tiffanie.lescure@gmail.com;

Abstract

Human exposure to heat stress is increasing under climate change as rising temperatures interact with atmospheric moisture to constrain thermoregulation and outdoor activity. While numerous heat-stress indices are used in climate impact studies, their joint interpretation in terms of climatic regimes, persistence, and physiological relevance remains fragmented. Here, we provide a global, multi-model assessment of future human-relevant heat stress using a consistent set of biometeorological indices derived from CMIP6 climate projections.

We analyse daily bias-corrected projections from the NASA NEX-GDDP-CMIP6 dataset at 0.25° resolution, using five CMIP6 models under SSP1–2.6, SSP2–4.5, and SSP5–8.5 scenarios. Wet-bulb temperature (Tw), wet-bulb globe temperature (WBGT), Heat Index, and Humidex are computed consistently and evaluated against ERA5 for the historical period. Heat stress is characterised through mean conditions, peak daily stress, and chronic threshold exceedance, defined as at least 30 days per year above physiologically and operationally relevant thresholds.

All indices indicate a robust intensification of heat stress under future warming, reflecting a systematic elevation of baseline thermal environments rather than isolated extremes. Under SSP5–8.5, more than five billion people are projected to experience at least one month per year with WBGT ≥ 32°C by late century, while over two billion may be exposed to chronic extreme humid heat (Tw ≥ 35°C). These exposures are concentrated in densely populated tropical and subtropical regions, particularly in Asia and Africa, and are substantially reduced under lower-emission pathways.

WBGT-based exceedance highlights expanding constraints on sustained outdoor activity, whereas extreme wet-bulb temperature represents a fundamental

atmospheric limit to evaporative cooling. By distinguishing between mean intensification, peak stress, and persistence-based exceedance across multiple indices, this study provides a climatologically grounded framework for assessing emerging heat-stress regimes relevant to applied climatology, climate services, and long-term adaptation planning.

Keywords: Heat stress; Biometeorology; Wet-bulb globe temperature (WBGT); Wet-bulb temperature; Climate projections; Chronic heat exposure

1 Introduction

Anthropogenic climate change is intensifying human exposure to heat stress through increases in both air temperature and atmospheric moisture, leading to more frequent, intense, and persistent heat–humidity extremes. Unlike many other climate hazards, extreme heat acts directly on human physiology, constraining thermoregulation, physical performance, and ultimately the feasibility of sustained outdoor activity. These constraints are governed by biophysical limits that cannot be fully mitigated through short-term behavioural adaptation once critical thresholds are exceeded.

A substantial body of physiological, occupational, and epidemiological research demonstrates that elevated heat stress impairs physical work capacity, increases cardiovascular and thermoregulatory strain, elevates dehydration risk, and raises the incidence of heat-related illness and mortality. Early syntheses identified heat stress as a growing occupational health challenge, particularly in low- and middle-income countries where outdoor labour is prevalent and adaptive capacity is limited (Kjellstrom, Holmer, & Lemke, 2009). Foundational work on human thermal environments established the physiological mechanisms linking environmental heat exposure to comfort, performance, and health outcomes (Parsons, 2006). More recent global health assessments confirm that extreme heat already affects a substantial fraction of the world's population and workforce, with risks projected to increase sharply under continued warming (Ebi, Capon, Berry, et al., 2021).

To characterise human heat stress in relation to physiology, a range of bioclimatic indices has been developed. These indices differ in complexity, required inputs, and physiological relevance, and include the heat index (HI), humidex, wet-bulb temperature (Tw), and wet-bulb globe temperature (WBGT). HI and humidex combine air temperature and humidity and are widely used in public health communication and epidemiological studies. For instance, heat index has been shown to be strongly associated with hydration status and health outcomes in contrasting hot-humid and hot-arid environments (Ebi et al., 2021; Kjellstrom et al., 2009). However, these indices do not explicitly account for solar radiation or wind, limiting their applicability for outdoor exposure and occupational risk assessment.

WBGT was specifically designed to represent the combined effects of air temperature, humidity, solar radiation, and wind on human heat strain. As a result, it has become the reference index in occupational health, military, and sports guidelines, and is embedded in international standards such as ISO 7243. Laboratory and field

studies demonstrate strong relationships between WBGT and reductions in physical work capacity across a wide range of environmental conditions (Foster, Smallcombe, Hodder, et al., 2021). At regional scales, WBGT-based analyses consistently show that rising temperatures are already pushing working conditions toward physiologically hazardous regimes, with severe implications for outdoor labour in South-East Asia, China, and the Middle East (**??**).

At the global scale, WBGT has been widely adopted in climate impact assessments linking warming to constraints on human activity. A seminal study by Dunne, Stouffer, and John (2013) demonstrated that increasing heat stress under climate warming could substantially reduce labour capacity across tropical and subtropical regions, highlighting physiological limits as a direct constraint on economic activity. Subsequent analyses using reanalysis data and climate model ensembles confirmed that exposure to extreme WBGT values is increasing rapidly with global mean temperature, and that population exposure to hazardous heat stress has already risen markedly over recent decades (Li, Yuan, & Kopp, 2020).

In parallel, wet-bulb temperature (Tw) has emerged as a fundamental physiological metric representing the theoretical lower bound of evaporative cooling. Sherwood and Huber (2010) proposed that a Tw of 35 °C constitutes an upper physiological boundary beyond which uncompensable heat stress would occur even for young, healthy individuals. Observational analyses have since shown that near-35 °C Tw values have already been recorded at a small number of coastal subtropical locations, and that extreme humid heat events have more than doubled in frequency since the late twentieth century (Raymond, Matthews, & Horton, 2020).

Recent experimental and physiology-based studies refine this interpretation. Controlled laboratory experiments demonstrate that uncompensable heat stress often occurs at Tw values substantially below 35 °C, depending on humidity, metabolic rate, and exposure conditions (Vecellio, Wolf, Cottle, & Kenney, 2022). More comprehensive physiological modelling further shows that reliance on a single universal Tw = 35 °C threshold can substantially underestimate heat risk, particularly for older adults and for sustained activity levels relevant to work and daily life (Vanos, Guzman-Echavarria, Baldwin, et al., 2023). These findings suggest that Tw = 35 °C should be interpreted as an extreme benchmark rather than a sharp universal physiological boundary.

Methodological uncertainties further complicate global heat stress assessments. Several studies rely on simplified or empirical approximations of WBGT due to data limitations. However, detailed evaluations demonstrate that such approximations can introduce systematic biases, particularly in hot-humid and hot-dry regimes, leading to substantial over- or under-estimation of extreme heat stress (**?**). Physically based formulations of WBGT derived from reanalysis data provide a more robust basis for large-scale assessments (Brimicombe, Lo, Pappenberger, et al., 2023; **?**). Instrumental studies further show that measurement choices related to globe temperature and mean radiant temperature can significantly affect WBGT estimates, underscoring the need for physically consistent approaches (**??**).

Despite this extensive literature, several gaps remain. Most global studies focus on the occurrence of extreme heat stress on individual days, while comparatively little attention has been paid to the persistence or duration of hazardous conditions, even

though prolonged exposure is likely to have more severe consequences for health, recovery, and habitability. Moreover, studies typically rely on a single heat stress index, despite evidence that different indices capture complementary dimensions of human heat strain and may diverge substantially under certain climatic regimes.

Here, we address these gaps by providing a global, multi-model assessment of human heat stress exposure based on an ensemble of five CMIP6 climate models from the NASA NEX-GDDP dataset at 0.25° spatial resolution. We explicitly compare multiple heat stress indices (WBGT, Tw, heat index, and humidex) to characterise their similarities and divergences across climatic regimes. We focus on two complementary and physiologically meaningful thresholds: WBGT $\geq$ 32 °C, commonly associated with severe reductions in physical work capacity, and Tw $\geq$ 35 °C, widely cited as a benchmark for extreme humid heat. Crucially, we adopt a duration-based perspective by identifying regions where these thresholds are exceeded for at least 30 days yr^{-1}, capturing the emergence of chronic extreme heat stress rather than isolated events. By quantifying the spatial extent and population exposure associated with these persistent co-exceedances, this work provides a robust, physiology-centred assessment of the climatic constraints on human activity under future warming.

2 Data and Methods

2.1 Climate projections (CMIP6 and NEX-GDDP-CMIP6, 0.25°)

We use daily bias-corrected and statistically downscaled CMIP6 projections from the NASA NEX-GDDP-CMIP6 archive at 0.25° spatial resolution. The original global climate simulations follow the CMIP6 experimental protocol (Eyring, Bony, Meehl, et al., 2016) under the ScenarioMIP framework (O'Neill et al., 2016). The NEX-GDDP-CMIP6 dataset applies Bias-Correction Spatial Disaggregation (BCSD) to produce inter-model harmonised projections suitable for climate impact analyses (Thrasher et al., 2022).

Previous evaluations indicate that raw CMIP6 models may exhibit biases in representing wet heatwave characteristics, including persistence and magnitude of wet-bulb temperature extremes (Zhao, Yin, & Hall, 2025). Bias correction in NEX-GDDP reduces mean biases but may not fully correct temporal autocorrelation structures of humid heat extremes (Zhao et al., 2025). These limitations are considered when interpreting projected threshold exceedances.

We analyse an ensemble of five CMIP6 models (GFDL-ESM4, IPSL-CM6A-LR, MRI-ESM2-0, MPI-ESM1-2-HR, and UKESM1-0-LL) under three emissions scenarios: SSP1–2.6, SSP2–4.5, and SSP5–8.5. Climate conditions are evaluated over 30-year periods: 1991–2020 (historical reference), 2041–2070 (mid-century), and 2071–2100 (late century). Multi-model ensemble means are analysed.

Daily near-surface air temperature (mean and maximum), relative humidity, wind speed, and downward shortwave radiation are used to derive heat-stress indices. No additional bias correction is applied beyond NEX-GDDP processing.

2.2 Reanalysis benchmark (ERA5)

To assess the plausibility of historical spatial patterns and magnitudes of heat-stress indices, we use the ERA5 reanalysis (Hersbach, Bell, Berrisford, et al., 2020). ERA5 provides a dynamically consistent global atmospheric reconstruction at high temporal resolution. ERA5 is analysed at 0.25° resolution for consistency with NEX-GDDP projections. It is treated as a physically coherent benchmark rather than observational ground truth.

2.3 Population projections and exposure assessment

Human exposure is quantified using gridded 1 km population projections consistent with the Shared Socioeconomic Pathways (O'Neill, Kriegler, Riahi, et al., 2014; O'Neill et al., 2016). We use the global population dataset of Wang, Meng, and Long (2022), harmonised with SSP trajectories.

Population and climate scenarios are treated in co-evolution: SSP-specific population projections are paired with their corresponding SSP climate forcing. Population counts are conservatively remapped to the 0.25° grid. Exposure is computed as the total population residing in grid cells exceeding defined heat-stress thresholds, following approaches similar to Mora, Dousset, Caldwell, et al. (2017).

2.4 Heat-stress indicators

Four bioclimatic indices are used: wet-bulb temperature (Tw), wet-bulb globe temperature (WBGT), humidex, and heat index (HI).

Wet-bulb temperature (Tw).

Tw is computed using the analytical approximation of Stull (2011). Wet-bulb temperature represents the theoretical lower bound of evaporative cooling and underpins physiological heat tolerance limits (Sherwood & Huber, 2010). Although Tw = 35°C has been proposed as an upper survivability benchmark (Sherwood & Huber, 2010), recent laboratory evidence indicates uncompensable heat stress may occur at lower values depending on activity and exposure duration (Vanos et al., 2023; Vecellio et al., 2022).

Wet-bulb globe temperature (WBGT).

WBGT is computed using the standard shade formulation:

$$\mathrm{WBGT}_{\mathrm{shade}} = 0.7\,T_w + 0.3\,T.$$

This formulation excludes direct solar radiation and is appropriate for shaded conditions. WBGT is widely used in occupational and athletic heat-stress guidelines and is strongly linked to reductions in physical work capacity (Dunne et al., 2013; Foster et al., 2021; Kjellstrom et al., 2009).

Humidex and Heat Index.

Humidex is calculated using the Canadian formulation based on vapour pressure. Heat Index (HI) is computed using the Rothfusz regression (Rothfusz, 1990). These

indices provide comparability with operational heat-warning systems and prior impact assessments.

2.5 Extreme heat metrics

Extreme exposure is characterised using daily maxima. Two primary thresholds are considered:

- WBGT $\geq$ 32 °C (severe occupational heat stress),
- Tw $\geq$ 35 °C (upper physiological benchmark).

To capture persistent exposure, we compute the annual number of days exceeding each threshold and identify regions with $\geq$30 days yr^{-1} exceedance. This chronic-exposure framing emphasises sustained thermal stress beyond isolated extreme events.

3 Results

3.1 Historical representation of heat-stress indices relative to ERA5

The historical spatial patterns of heat-stress indices simulated by the NEX-GDDP-CMIP6 ensemble were evaluated against the ERA5 reanalysis over the 1991–2020 period (Fig. 1). ERA5 is used here as a physically consistent benchmark rather than as an observational reference.

For all indices, the ensemble-mean differences relative to ERA5 remain moderate at the global scale, with no evidence of systematic large-scale bias. Spatial patterns of bias are regionally structured and broadly consistent across indices, with larger deviations occurring primarily in regions characterised by strong humidity gradients and complex near-surface climate regimes, including parts of the tropics and subtropics.

Wet-bulb temperature and WBGT show similar large-scale bias structures, reflecting their shared dependence on temperature and atmospheric moisture. Heat Index and Humidex exhibit locally stronger positive biases in hot and humid regions, consistent with their formulation and sensitivity to humidity under high-temperature conditions. In mid- and high-latitude regions, biases are generally weak and spatially smooth across all indices.

Overall, the comparison indicates that the NEX-GDDP-CMIP6 ensemble reproduces the broad spatial distribution and magnitude of historical heat-stress conditions with sufficient physical consistency to support its use for future regime and persistence analyses. Inter-model ranges for mean WBGT and Tw over the historical reference period are shown in Supplementary Fig. A1.

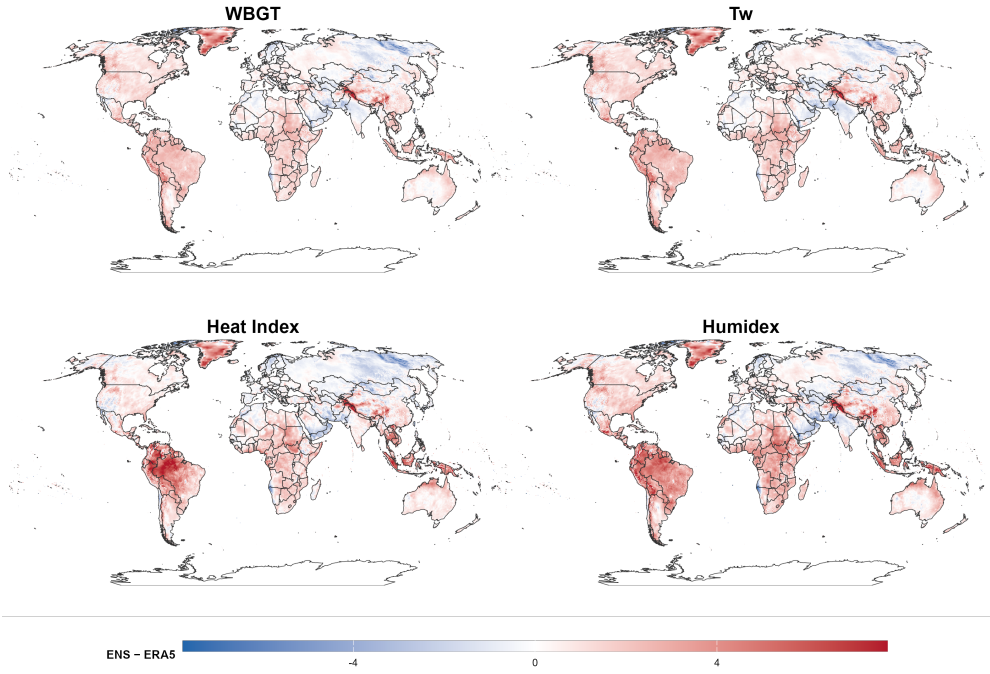

Fig. 1 Spatial bias of historical heat-stress indices (ensemble mean of NEX-GDDP-CMIP6 minus ERA5) over the 1991–2020 period at 0.25° resolution. ERA5 is used as a physically consistent benchmark. Bias patterns are shown for WBGT, wet-bulb temperature (Tw), Heat Index, and Humidex.

3.2 Mean annual heat-stress indices under future climate scenarios

Figure 2 shows the spatial distribution of mean annual heat-stress indices for wet-bulb globe temperature (WBGT), wet-bulb temperature (Tw), Heat Index, and Humidex, computed from daily mean near-surface air temperature and averaged over the year. Results are shown for present-day conditions (1991–2020) and for the end-of-century period under SSP5–8.5.

All four indices exhibit a robust increase in mean annual values under future warming, with a clear amplification of heat stress across most land regions. Despite differences in formulation, the large-scale spatial patterns are broadly consistent among indices, with highest values concentrated in tropical and subtropical regions and lower values at higher latitudes. This agreement reflects the dominant role of large-scale temperature and humidity changes in shaping mean human-relevant thermal conditions.

Notable regional differences among indices are nevertheless apparent. Heat Index and Humidex tend to show stronger increases in humid tropical regions, consistent with their formulation and sensitivity to atmospheric moisture. WBGT and Tw display

smoother spatial gradients and comparatively more moderate increases in some arid regions, reflecting the limiting influence of lower humidity on evaporative processes.

Overall, the use of daily mean temperature highlights a widespread intensification of the baseline thermal environment rather than isolated extreme conditions. This provides a complementary perspective to peak-based analyses, illustrating how future climate change progressively elevates the average level of heat stress experienced throughout the year. The other scenarios (SSP1-2.6 et SSP2-4.5) are available the Supplementary Information. These mean-condition patterns provide context for the peak-based and threshold-focused analyses presented in the following sections, which address the emergence of extreme and chronic heat-stress constraints.

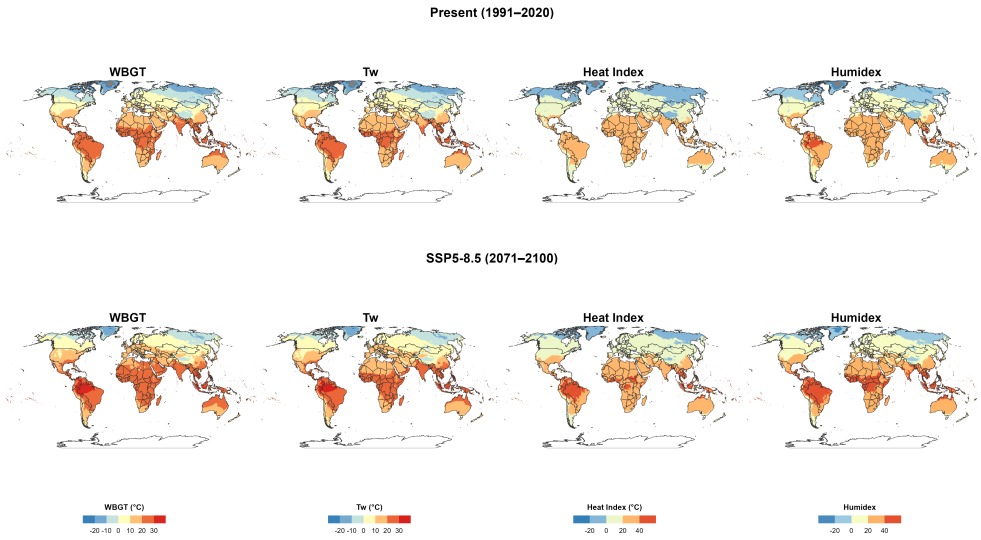

Fig. 2 Mean annual heat-stress indices for WBGT, wet-bulb temperature (Tw), Heat Index, and Humidex under present-day conditions (1991–2020) and end-of-century climate (2071–2100, SSP5–8.5). Indices are computed from daily mean near-surface air temperature and averaged over the year, highlighting large-scale changes in baseline thermal stress.

3.3 Mean peak heat-stress indices derived from daily maximum temperature

Figure 3 shows the spatial distribution of mean peak heat-stress indices for wet-bulb globe temperature (WBGT) and wet-bulb temperature (Tw), computed from daily maximum near-surface air temperature and averaged over the year. Results are shown for the historical period (1991–2020) and for end-of-century conditions under SSP5–8.5 (2071–2100).

Compared to mean-condition indices derived from daily average temperature, peak-based WBGT and Tw values are systematically higher and exhibit sharper spatial gradients. Under present-day conditions, high peak values are already evident across

large parts of the tropics and subtropics, reflecting the combined influence of high daytime temperatures and atmospheric moisture during the warm season.

Under SSP5–8.5, mean peak WBGT and Tw intensify substantially and expand poleward, particularly across subtropical regions. Increases are not limited to regions already experiencing high heat stress, but also affect areas currently characterised by moderate peak conditions, indicating a broad amplification of daytime thermal extremes. The contrast between low- and high-latitude regions remains pronounced, but the overall distribution shifts toward higher peak stress levels across most land areas. Peak heat-stress patterns under SSP1–2.6 and SSP2–4.5 are shown in Supplementary Fig. A2 and A3.

These peak-based patterns highlight the importance of daytime maximum conditions in shaping future human-relevant heat stress, providing a necessary bridge between mean climate changes and threshold-based analyses of extreme and chronic exposure. While these peak-based indices characterise the intensification of daytime heat stress, they do not directly indicate how often critical thresholds are exceeded, which is addressed in the following section.

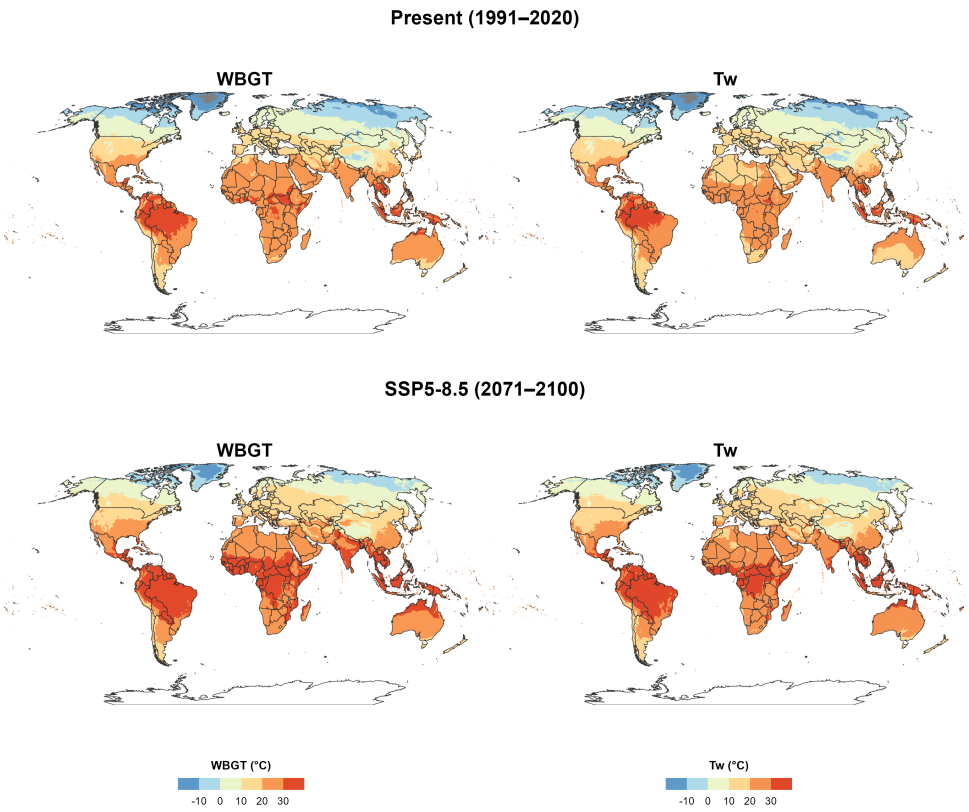

Fig. 3 Mean peak wet-bulb globe temperature (WBGT) and wet-bulb temperature (Tw) under present-day climate (1991–2020) and end-of-century conditions (2071–2100, SSP5–8.5). Indices are computed from daily maximum near-surface air temperature and averaged over the year, highlighting changes in daytime peak heat stress.

3.4 Chronic exceedance of physiological and work-relevant heat-stress thresholds under SSP5–8.5

Figure 4 shows regions experiencing chronic exceedance of two critical heat-stress thresholds, defined here as at least 30 days per year above Tw $\geq$ 35 °C and WBGT $\geq$ 32 °C, for the historical period (1991–2020), mid-century (2031–2060), and end-of-century (2071–2100) under SSP5–8.5.

Under present-day conditions, chronic exceedance of Tw $\geq$ 35 °C is virtually absent at the global scale, while WBGT $\geq$ 32 °C already affects several regions, primarily in tropical and subtropical climates. These areas include parts of northern South America, sub-Saharan Africa, South and Southeast Asia, and northern Australia.

By mid-century, chronic exceedance of WBGT $\geq$ 32 °C expands substantially in both spatial extent and continuity, affecting large portions of the tropics and extending

into adjacent subtropical regions. In contrast, Tw $\geq$ 35 °C remains geographically limited but begins to emerge in distinct hotspots, particularly in parts of South America, West Africa, South Asia, and Southeast Asia.

By the end of the century, chronic exposure to WBGT $\geq$ 32 °C becomes widespread across most tropical land areas and several subtropical regions. At the same time, chronic exceedance of Tw $\geq$ 35 °C expands markedly, forming contiguous regions of extreme humid heat in parts of South America, Africa, South Asia, and Southeast Asia. These patterns indicate a clear divergence between widespread work-relevant heat-stress constraints and more spatially confined but physiologically extreme humid heat conditions. While these results illustrate the emergence of chronic heat-stress constraints under a high-emission scenario, the degree to which physiological and work-relevant thresholds co-occur and differ across emission pathways is examined in the following section. Chronic exceedance under SSP1–2.6 and SSP2–4.5 is shown in Supplementary Fig. A4 and A5.

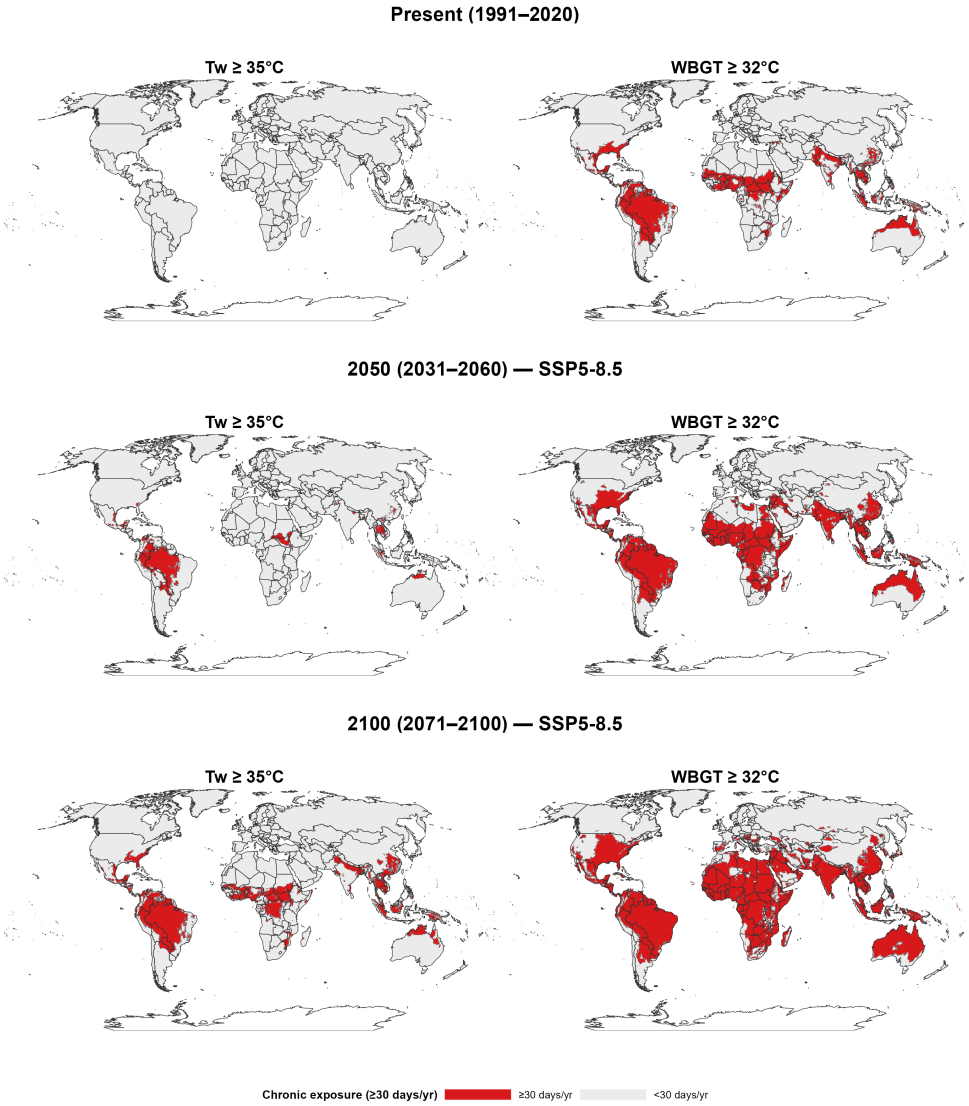

Fig. 4 Regions experiencing chronic exceedance of critical heat-stress thresholds, defined as at least 30 days per year above Tw $\geq$ 35 °C (left panels) and WBGT $\geq$ 32 °C (right panels), for the present climate (1991–2020), mid-century (2031–2060), and end-of-century (2071–2100) under SSP5–8.5. Chronic exposure highlights the emergence of persistent physiological and work-relevant heat-stress regimes.

3.5 Co-occurrence of chronic physiological and work-relevant heat-stress constraints across SSPs

Figure 5 shows the spatial distribution of regions experiencing co-occurring chronic exceedance of both Tw $\geq$ 35 °C and WBGT $\geq$ 32 °C, defined as at least 30 days per year above both thresholds. Results are presented for mid-century (2031–2060) and end-of-century (2071–2100) periods under SSP1–2.6, SSP2–4.5, and SSP5–8.5.

Across all scenarios, co-occurrence of chronic exceedance remains geographically limited compared to WBGT exceedance alone, reflecting the more restrictive nature of the extreme humid heat constraint imposed by Tw. Regions identified in this analysis therefore correspond to environments where physiological limits on evaporative cooling coincide with sustained work-relevant heat stress.

By mid-century, co-occurring chronic exposure emerges only in a small number of regional hotspots, primarily in parts of northern South America and Southeast Asia, with limited sensitivity to emission scenario. Differences among SSPs remain modest at this time horizon, indicating that the most extreme combined constraints are not yet widespread.

By the end of the century, scenario dependence becomes pronounced. Under SSP1–2.6, co-occurring chronic exceedance remains rare and spatially fragmented. Under SSP2–4.5, affected regions expand in extent and continuity, particularly in tropical South America. Under SSP5–8.5, co-occurring chronic exposure increases markedly, forming larger contiguous regions across parts of South America, Africa, South Asia, and Southeast Asia.

These results indicate that the co-occurrence of physiological and operational heat-stress constraints is primarily controlled by the emergence of extreme humid heat conditions, with emission pathways strongly modulating the spatial extent and severity of combined constraints at longer time horizons. The population exposure associated with these co-occurring chronic heat-stress regimes is quantified in the following section.

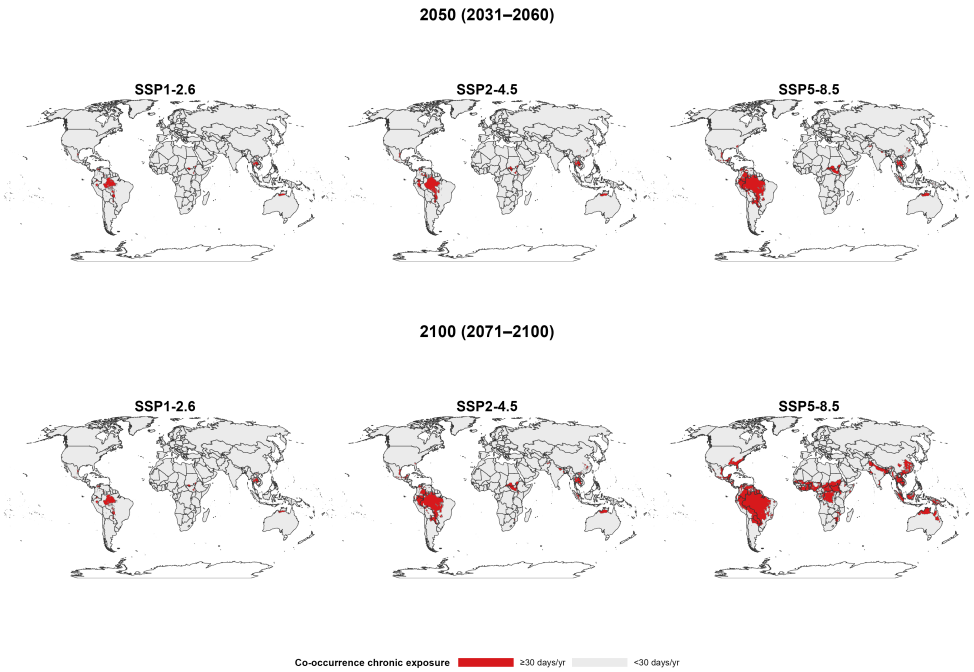

Fig. 5 Regions experiencing co-occurring chronic exceedance of Tw $\geq$ 35 °C and WBGT $\geq$ 32 °C, defined as at least 30 days per year above both thresholds, for mid-century (2031–2060) and end-of-century (2071–2100) periods under SSP1–2.6, SSP2–4.5, and SSP5–8.5. Co-occurrence highlights environments where extreme humid heat constrains both physiological tolerance and sustained outdoor activity.

3.6 Population exposure to chronic extreme heat-stress regimes

Table 1 quantifies population exposure to chronic extreme heat stress, defined as at least 30 days per year exceeding either Tw $\geq$ 35 °C or WBGT $\geq$ 32 °C, for mid-century (2041–2070) and end-of-century (2071–2100) periods under SSP1–2.6, SSP2–4.5, and SSP5–8.5. Population exposure is computed using SSP-consistent gridded population projections aggregated at continental and global scales. Values are reported in billions of people with ensemble ranges.

At the global scale, exposure to WBGT $\geq$ 32 °C is substantially larger than exposure to Tw $\geq$ 35 °C across all scenarios and periods. Under SSP5–8.5, 5.66 billion people are exposed to chronic WBGT exceedance by mid-century, increasing slightly to 5.95 billion by 2071–2100. Under SSP2–4.5, exposure reaches 6.17 billion by late century, while under SSP1–2.6 it remains below 4 billion.

In contrast, global exposure to Tw $\geq$ 35 °C remains limited through mid-century (0.44 billion under SSP5–8.5) but increases sharply to 2.44 billion by 2071–2100 under

the high-emission scenario. Under SSP2–4.5, late-century exposure reaches 0.53 billion, while it remains below 0.1 billion under SSP1–2.6.

Regional patterns are strongly heterogeneous. Asia consistently accounts for the largest exposed population for both metrics, reflecting the combination of high baseline heat stress and large population totals. Under SSP5–8.5, 1.51 billion people in Asia are exposed to chronic Tw $\geq$ 35 °C by late century, compared with 0.67 billion in Africa. Africa exhibits a particularly strong relative increase in exposure to extreme humid heat, rising from 0.04 billion mid-century to 0.67 billion by 2071–2100 under SSP5–8.5.

Exposure to WBGT $\geq$ 32 °C is widespread across all major regions. By late century under SSP5–8.5, 3.14 billion people in Asia and 1.68 billion in Africa experience chronic WBGT exceedance, with additional exposure in North America (0.75 billion) and South America (0.23 billion). Europe and Oceania remain comparatively less affected in absolute terms, although exposure increases under higher-emission pathways.

Because chronic co-occurrence of WBGT $\geq$ 32 °C and Tw $\geq$ 35 °C is controlled by the more restrictive Tw threshold, population exposure to co-occurring chronic constraints is equivalent to the Tw $\geq$ 35 °C estimates reported above.

Ensemble ranges indicate substantial inter-model spread for extreme humid heat, particularly under SSP5–8.5, where global Tw $\geq$ 35 °C exposure spans 0.21–4.11 billion by late century. In contrast, uncertainty ranges for WBGT exposure are proportionally narrower, although still non-negligible at continental scales. These ranges highlight structural model uncertainty in the spatial extent and persistence of extreme humid heat.

4 Discussion

4.1 From episodic extremes to structural climatic constraint

Most assessments of heat-related climate risk focus on isolated extreme events. Our results instead highlight the emergence of a structural climatic regime in which physiologically stressful conditions persist for weeks each year. This regime framing is consistent with evidence that climate change alters not only heat intensity but also frequency, duration, and persistence (Li et al., 2020; Matthews, Wilby, & Murphy, 2017; Perkins & Alexander, 2013; Raymond et al., 2020).

Under SSP5–8.5, approximately 5.7 billion people are exposed to chronic WBGT $\geq$ 32 °C by mid-century, increasing to nearly 6.0 billion by late century. For extreme humid heat (Tw $\geq$ 35 °C), exposure increases to 2.44 billion people by 2071–2100 under SSP5–8.5. These magnitudes fundamentally shift the interpretation of humid heat from localized hazard to systemic climatic constraint. Differences between SSP2–4.5 and SSP5–8.5 partly reflect contrasting demographic trajectories embedded in the SSP framework, rather than purely climatic differences.

Ensemble ranges reported in Table 1 indicate substantial inter-model spread, particularly for extreme humid heat. Under SSP5–8.5 late century, global exposure to chronic Tw $\geq$ 35 °C spans 0.21–4.11 billion people across ensemble members. This spread reflects sensitivity to small differences in temperature–humidity coupling and persistence characteristics among models. In contrast, WBGT-based exposure exhibits

Table 1 Population exposed to chronic extreme humid heat conditions (billions of people). Exposure is defined as at least 30 days per year exceeding the specified threshold. Values are reported as ensemble mean with ensemble range in brackets (ensmin–ensmax).

Region	**Metric**	**SSP1–2.6**		**SSP2–4.5**		**SSP5–8.5**	
		2041–2070	2071–2100	2041–2070	2071–2100	2041–2070	2071–2100
Global	**$Tw_{\geq 35}$**	0.088 [0.001–0.539]	0.066 [0.001–0.618]	0.153 [0.002–1.118]	0.525 [0.009–2.197]	0.442 [0.013–2.276]	2.443 [0.212–4.114]
Global	**$WBGT_{\geq 32}$**	4.724 [2.826–5.821]	3.827 [2.246–4.748]	5.607 [3.672–6.746]	6.169 [4.531–7.235]	5.662 [3.935–6.824]	5.954 [4.489–7.053]
Africa	$Tw_{\geq 35}$	0.007 [0.000–0.053]	0.008 [0.000–0.050]	0.015 [0.000–0.080]	0.038 [0.001–0.545]	0.037 [0.001–0.432]	0.671 [0.016–1.180]
Africa	$WBGT_{\geq 32}$	1.050 [0.564–1.270]	1.169 [0.620–1.413]	1.305 [0.822–1.552]	1.954 [1.414–2.269]	1.257 [0.798–1.479]	1.680 [1.307–1.849]
Asia	$Tw_{\geq 35}$	0.062 [0.000–0.406]	0.045 [0.000–0.501]	0.103 [0.001–0.911]	0.414 [0.003–1.444]	0.331 [0.007–1.622]	1.512 [0.147–2.335]
Asia	$WBGT_{\geq 32}$	3.218 [2.042–3.891]	2.249 [1.443–2.733]	3.773 [2.565–4.437]	3.577 [2.745–4.030]	3.754 [2.760–4.340]	3.137 [2.544–3.479]
Europe	$Tw_{\geq 35}$	0.000 [0.000–0.000]	0.000 [0.000–0.000]	0.000 [0.000–0.000]	0.000 [0.000–0.000]	0.000 [0.000–0.000]	0.000 [0.000–0.001]
Europe	$WBGT_{\geq 32}$	0.001 [0.000–0.013]	0.000 [0.000–0.010]	0.001 [0.000–0.026]	0.006 [0.000–0.076]	0.008 [0.000–0.107]	0.124 [0.010–0.481]
North America	$Tw_{\geq 35}$	0.003 [0.000–0.024]	0.003 [0.000–0.025]	0.007 [0.001–0.045]	0.019 [0.002–0.095]	0.018 [0.002–0.106]	0.153 [0.013–0.424]
North America	$WBGT_{\geq 32}$	0.253 [0.108–0.361]	0.267 [0.101–0.390]	0.282 [0.148–0.408]	0.371 [0.220–0.531]	0.370 [0.220–0.553]	0.751 [0.442–0.925]
Oceania	$Tw_{\geq 35}$	0.000 [0.000–0.001]	0.000 [0.000–0.001]	0.001 [0.000–0.001]	0.001 [0.000–0.002]	0.001 [0.000–0.002]	0.003 [0.001–0.008]
Oceania	$WBGT_{\geq 32}$	0.007 [0.003–0.011]	0.006 [0.002–0.011]	0.008 [0.004–0.013]	0.012 [0.006–0.020]	0.010 [0.005–0.019]	0.026 [0.011–0.053]
South America	$Tw_{\geq 35}$	0.015 [0.000–0.056]	0.011 [0.000–0.043]	0.027 [0.000–0.080]	0.052 [0.003–0.110]	0.055 [0.003–0.113]	0.104 [0.035–0.166]
South America	$WBGT_{\geq 32}$	0.194 [0.109–0.274]	0.135 [0.080–0.192]	0.237 [0.133–0.309]	0.248 [0.146–0.308]	0.262 [0.152–0.326]	0.235 [0.175–0.264]

comparatively narrower relative ranges, suggesting greater robustness of work-relevant threshold exceedance relative to the most physiologically extreme humid-heat regime. These uncertainties should therefore be interpreted as structural model uncertainty rather than statistical sampling error.

Recent observational analyses confirm that extreme humid heat has intensified more rapidly than previously estimated, with localized Tw values approaching 35 °C already observed in subtropical regions (Raymond et al., 2020). Our projections suggest that such conditions may become recurrent seasonal features across densely populated tropical and subtropical belts.

Importantly, exposure is unevenly distributed. Asia and Africa account for the largest increases, with over 1.3 billion people exposed to chronic Tw $\geq$ 35 °C in Asia and nearly 600 million in Africa under SSP5–8.5. These regions combine demographic growth with substantial dependence on outdoor labour and limited adaptive infrastructure, amplifying vulnerability (Ebi et al., 2021).

4.2 Implications for labour capacity, health, and development

WBGT is widely used as an operational metric of occupational heat stress and is embedded in international guidance (ISO 7243) (ISO, 2017). Seminal modelling work demonstrated that rising WBGT can substantially constrain global labour capacity (Dunne et al., 2013), and occupational syntheses highlight that heat stress is already an increasing challenge for health and productivity in low- and middle-income countries (Ebi et al., 2021; Kjellstrom et al., 2009). Experimental evidence confirms robust reductions in sustained work capacity as WBGT increases (Foster et al., 2021).

Chronic exceedance of WBGT $\geq$ 32 °C therefore represents more than discomfort: it signals structural constraints on agricultural productivity, construction work, and informal-sector labour. Field studies in tropical settings show measurable productivity impacts in heat-exposed workers and strong modulation by seasonal persistence rather than isolated daily maxima (Sahu, Sett, & Kjellstrom, 2013; Simpson, Hosking, Mitchell, Betts, & Shuckburgh, 2021). Empirical assessments of labour productivity and supply under climate change further indicate that these constraints can affect both effective labour supply and work intensity (Dasgupta et al., 2021).

Under lower-emission pathways, the scale and geographical extent of chronic exposure are reduced, highlighting the strong sensitivity of labour-relevant humid heat constraints to mitigation trajectories.

4.3 Physiological interpretation of Tw thresholds

The Tw $\geq$ 35 °C benchmark has often been cited as a theoretical upper limit for human heat tolerance (Sherwood & Huber, 2010). However, empirical chamber experiments show that uncompensable heat stress in healthy adults can occur at substantially lower wet-bulb temperatures, often near 30–31 °C in humid environments (Vecellio et al., 2022). Physiology-based modelling further demonstrates that survivability and liveability thresholds vary with age, radiation exposure, and metabolic rate (Vanos et

al., 2023). Consequently, the chronic exceedance patterns identified here likely represent conservative estimates of physiological risk, with functional limitations and health impacts emerging below the 35 °C benchmark (Ebi et al., 2021; Matthews et al., 2017).

4.4 Representation of humid heat in bias-corrected projections

We rely on the NASA NEX-GDDP-CMIP6 dataset (Thrasher et al., 2022), which applies bias-correction and spatial disaggregation to CMIP6 simulations. While such products reduce mean-state biases and are widely used for impact assessment, recent evaluations indicate that wet heatwave persistence and temporal clustering may not be perfectly reproduced even after bias correction (Zhao et al., 2025). This matters because humid-heat impacts depend not only on peak magnitude but also on multi-day clustering and recovery opportunities.

Our persistence-based exceedance metric ($\geq$30 days per year) partly mitigates this limitation by focusing on cumulative seasonal exposure rather than isolated peak events. Nonetheless, uncertainties in the temporal structure of humid heat extremes remain an important caveat, and the historical overestimation identified in Fig. 1 provides a concrete motivation to interpret late-century chronic exceedance as a screening indicator rather than a precise forecast.

4.5 Limitations of simplified WBGT formulations

The WBGT formulation used here corresponds to the standard shade approximation ($0.7\mathrm{Tw} + 0.3\mathrm{T}$) aligned with occupational screening applications (Parsons, 2006). This also the ISO7243 reference(ISO, 2017). This approach omits explicit globe temperature modelling and detailed radiative and convective heat exchange. Recent analyses show that simplified WBGT approximations can overestimate heat stress in hot–humid regions and underestimate it in hot–dry climates compared with physically explicit calculations (Kong & Huber, 2022). Furthermore, interactions between air velocity, humidity, clothing, and solar radiation are not fully captured by simplified indices (Foster et al., 2022,?).

Given the coarse resolution of global climate projections, the simplified shade formulation provides a consistent proxy for large-scale comparative analysis. Results should therefore be interpreted as order-of-magnitude estimates of climatic constraint rather than precise operational WBGT forecasts.

4.6 Chronic exceedance as structural transformation

By focusing on regions exceeding critical thresholds for at least 30 days per year, we move beyond event-based hazard framing toward a regime-based perspective. Chronic exceedance limits physiological recovery, increases cumulative strain, and transforms seasonal heat stress into a recurring structural constraint (Ebi et al., 2021; Kjellstrom et al., 2009). Such conditions do not imply immediate uninhabitability; rather, they signal progressive reductions in work feasibility, increased adaptation costs, and growing reliance on technological cooling and behavioural adjustments. This transformation is particularly consequential for regions with limited adaptive capacity and high dependence on outdoor labour (Dasgupta et al., 2021; Kjellstrom et al., 2009).

4.7 Implications for applied climatology and climate services

By integrating multi-model projections, SSP-consistent population co-evolution, and persistence-based exceedance metrics across multiple indices, this study reframes extreme humid heat as a systemic climatic constraint with large-scale societal implications. The scale of projected exposure — billions under high-emission scenarios — underscores that humid heat is not a marginal risk but a central component of future human climate experience.

Operational translation frameworks increasingly rely on WBGT-aligned exposure estimates by job and region, including heat job-exposure matrices that enable linkage between climate indicators and occupational risk assessment (de Crom et al., 2026). Global gridded WBGT products further support the development of climate services and early-warning contexts (Brimicombe et al., 2023). Applied climatology must therefore increasingly integrate physiologically grounded thresholds with demographic trajectories to inform adaptation planning, labour regulation, and long-term development strategies.

5 Conclusions

This study provides a global, multi-model assessment of future human-relevant heat stress using a consistent set of biometeorological indices derived from CMIP6 climate projections at 0.25° resolution. By jointly analysing wet-bulb temperature, wet-bulb globe temperature, Heat Index, and Humidex, and by explicitly accounting for the duration of threshold exceedance, we characterise how climate change alters not only the intensity but also the persistence of thermal constraints on human activity.

Our results indicate that under high-emission scenarios, more than five billion people may experience at least one month per year with WBGT ≥ 32°C by late century, while over two billion could be exposed to chronic extreme humid heat (Tw ≥ 35°C). These exposures are not uniformly distributed, but increasingly concentrate in densely populated tropical and subtropical regions, particularly in Asia and Africa.

Beyond general intensification, the emergence of chronic exceedance regimes marks a transition from episodic heat stress to persistent climatic constraint. WBGT-based exceedance highlights widespread and expanding limitations on sustained outdoor activity, including regions not traditionally considered heat-vulnerable, while extreme wet-bulb temperature remains more geographically confined but represents a fundamental atmospheric constraint on evaporative cooling.

The co-occurrence of chronic WBGT and extreme wet-bulb temperature exceedance identifies regions where both operational adaptation and physiological tolerance are simultaneously challenged. Differences across emission pathways demonstrate that the scale of chronic exposure is strongly sensitive to mitigation trajectories.

Rather than translating heat-stress metrics into direct productivity or economic impacts, this work frames exceedance as a climatological indicator of biophysical feasibility. In doing so, it provides a reproducible basis for identifying emerging heat-stress regimes relevant to applied climatology, climate services, labour regulation, and long-term adaptation planning.

Future research should integrate higher temporal resolution, urban and microclimatic processes, and vulnerability-sensitive exposure metrics to refine assessments of human heat stress. Nevertheless, the persistence-based framework presented here highlights that humid heat is likely to become a defining feature of the 21st-century human climate experience.

Supplementary information. If your article has accompanying supplementary file/s please state so here.

Authors reporting data from electrophoretic gels and blots should supply the full unprocessed scans for key as part of their Supplementary information. This may be requested by the editorial team/s if it is missing.

Please refer to Journal-level guidance for any specific requirements.

Acknowledgements

The author thanks the developers and data providers of the CMIP6 models, the NASA NEX-GDDP data archive. All computations were carried out using open-source software on the author's own computing resources.

Declarations

- Funding: Part of this research has been funded by the French Ministry of Foreign Affairs through its funding of the FSP AGRICORA programme.
- Conflict of interest/Competing interests : The authors declare no confliect of interest for this work.
- Data availability : All data used in this study are publicly available. Bias-corrected CMIP6 climate projections were obtained from the NASA NEX-GDDP dataset. All processed indicators and scripts used to generate the results will be made publicly available upon publication via Zenodo and GitHub.
- Author contribution : **TL**: Conceptualization; Methodology; Data curation; Formal analysis; Visualization; Writing – original draft. **DD.**: Investigation; Validation; Writing – review & editing.

If any of the sections are not relevant to your manuscript, please include the heading and write 'Not applicable' for that section.

This Supplementary Information provides additional figures and tables supporting the main manuscript. Supplementary Fig. S1 documents the inter-model range (ensemble max–min) of mean heat-stress indices for the historical reference period. Supplementary Fig. S3 and Fig. S4 report results under SSP1–2.6 and SSP2–4.5 for peak conditions and chronic exceedance, respectively, complementing the main-text focus on SSP5–8.5. Supplementary Table S1 reports population exposure ranges based on ensemble mean, minimum, and maximum estimates.

Appendix A Supplementary figures

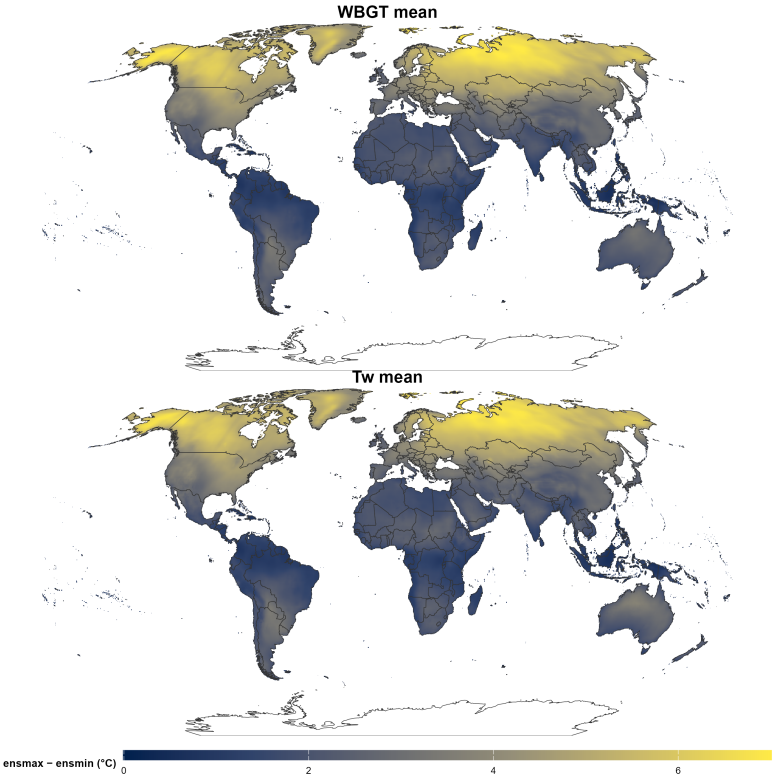

Fig. A1 Inter-model range of mean heat-stress indices for the historical reference period (1991–2020). Maps show the ensemble range computed as ensemble maximum minus ensemble minimum (ensmax–ensmin) for (a) mean WBGT (shade formulation) and (b) mean wet-bulb temperature (Tw). Both indices are derived consistently from the NEX-GDDP-CMIP6 daily projections aggregated to climatological means. The inter-model range highlights spatial heterogeneity in model spread, with larger ranges typically occurring in hot and humid regions where small differences in humidity and temperature can strongly influence derived heat-stress metrics.

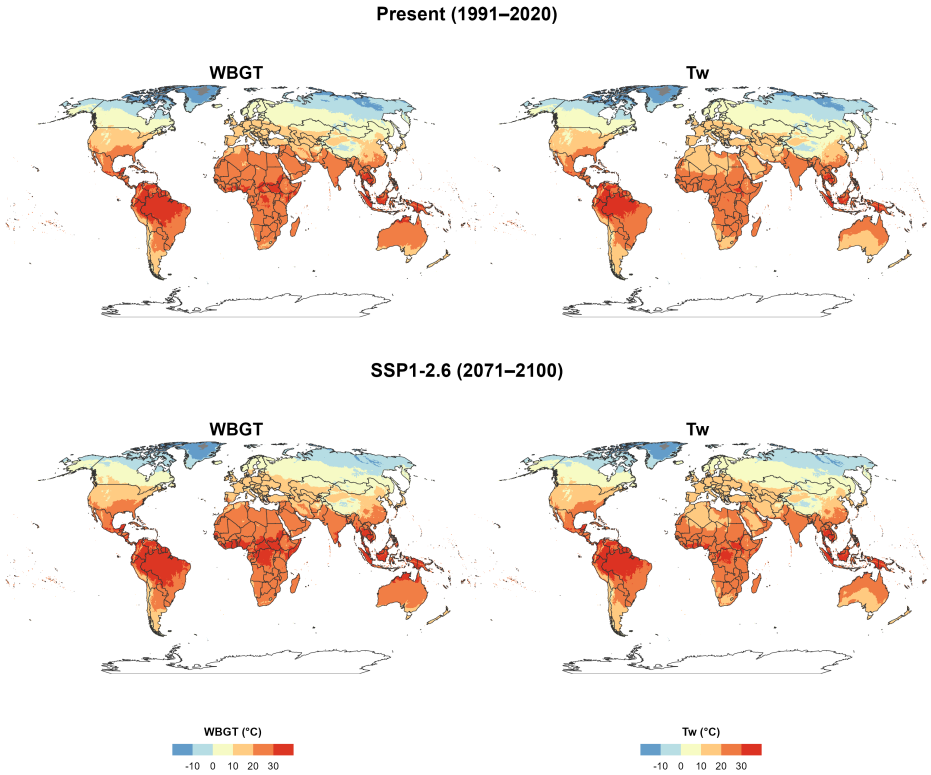

Fig. A2 Peak heat-stress climatologies under SSP1–2.6. Panels show present-day (1991–2020) and late-century (2071–2100) climatologies of peak indices estimated from daily maximum conditions, consistent with the main-text definition. The figure complements the SSP5–8.5 results in the main manuscript by illustrating the magnitude and spatial structure of peak heat stress under a low-emission pathway.

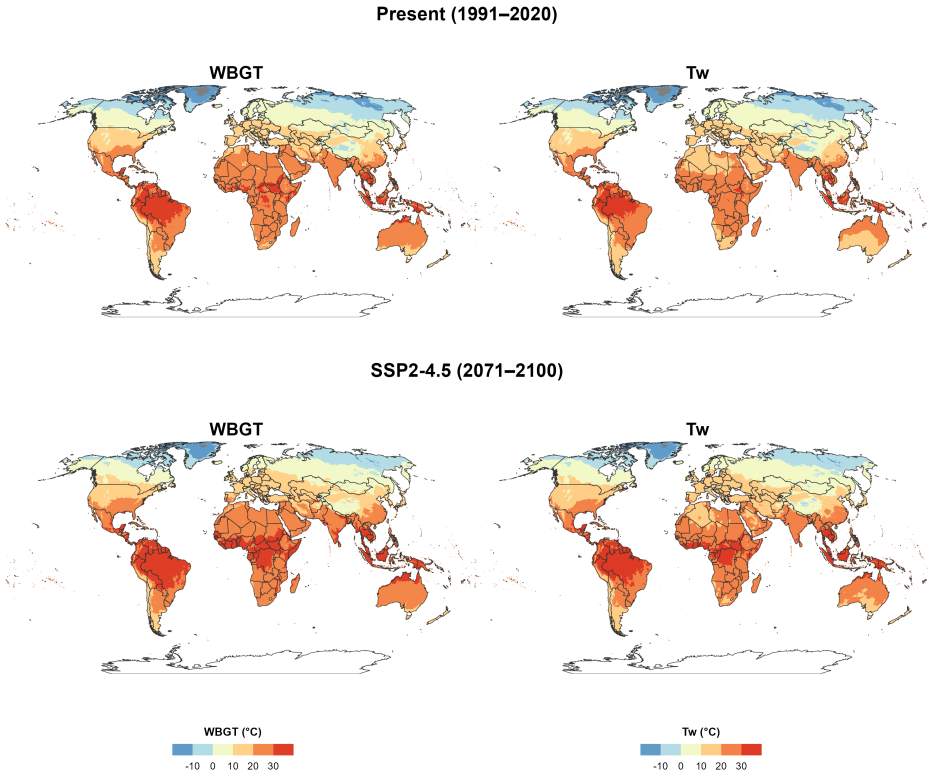

Fig. A3 Peak heat-stress climatologies under SSP2–4.5. Same as Supplementary Fig. S3a but for the intermediate-emissions scenario SSP2–4.5.

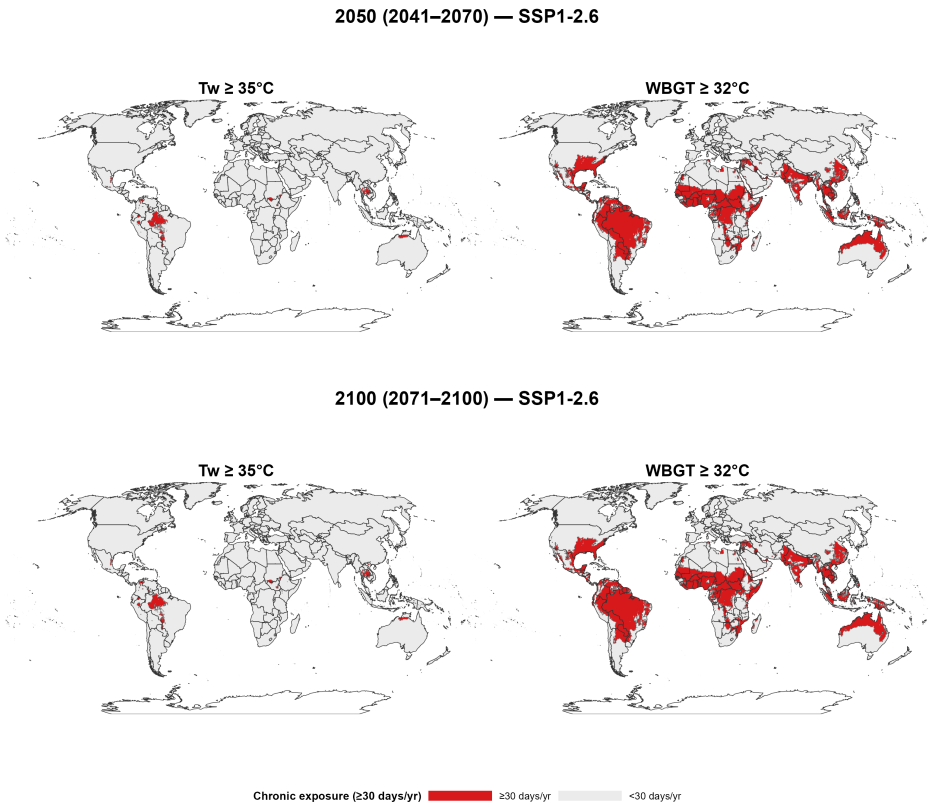

Fig. A4 Chronic exceedance of heat-stress thresholds under SSP1–2.6. Maps show regions where thresholds are exceeded for at least 30 days yr^{-1} for mid-century (2041–2070) and late-century (2071–2100). Panels report chronic exceedance for Tw $\geq 35°C$ and WBGT (shade) $\geq 32°C$ following the main-text definition. This figure complements the SSP5–8.5 maps in the main manuscript by illustrating the reduction in chronic exceedance under strong mitigation.

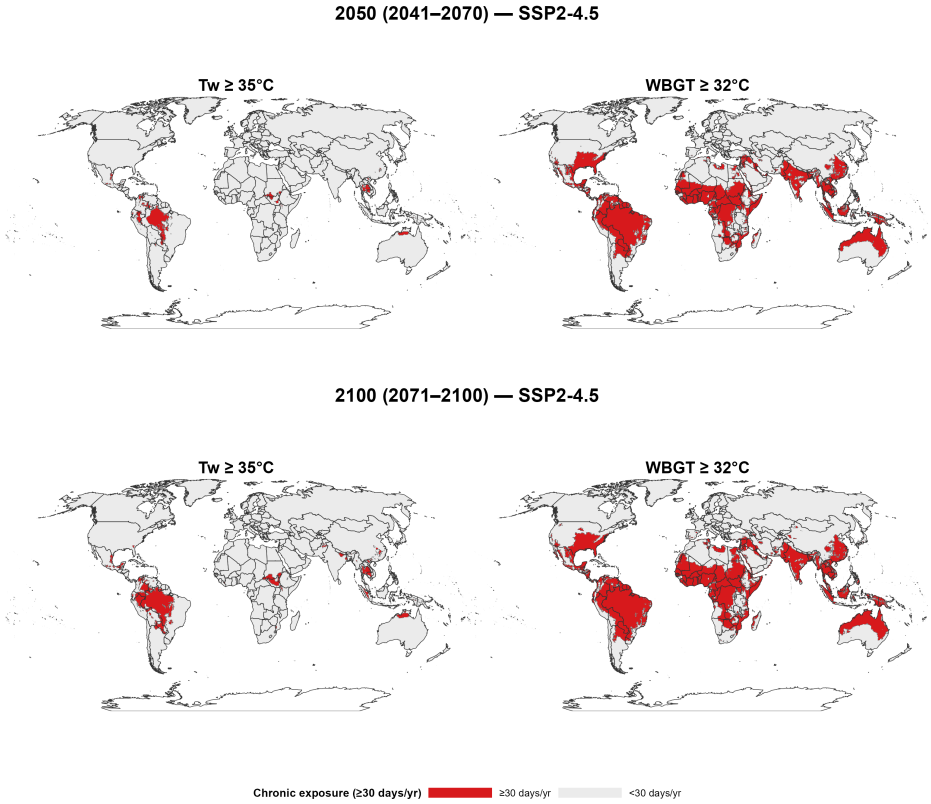

Fig. A5 Chronic exceedance of heat-stress thresholds under SSP2–4.5. Same as Supplementary Fig. S4a but for SSP2–4.5.

References

Brimicombe, C., Lo, C.H.B., Pappenberger, F., et al. (2023). Wet bulb globe temperature: Indicating extreme heat risk on a global grid. *GeoHealth*, *7*(2), e2022GH000701, https://doi.org/10.1029/2022GH000701

Dasgupta, S., van Maanen, N., Gosling, S.N., Piontek, F., Otto, C., Schleussner, C.-F. (2021). Effects of climate change on combined labour productivity and supply: an empirical, multi-model study. *The Lancet Planetary Health*, *5*(7), e455–e465, https://doi.org/10.1016/S2542-5196(21)00170-4

de Crom, T.O., Scholten, B., Traini, E., van der Sanden, K., Kingma, B., Pekel, F., ... Pronk, A. (2026, Jan). Exposure to heat at work: development of a quantitative european job exposure matrix (heat jem). *Scandinavian Journal of Work, Environment Health*, *52*(1), 7–18, https://doi.org/10.5271/sjweh.4243

Dunne, J.P., Stouffer, R.J., John, J.G. (2013). Reductions in labour capacity from heat stress under climate warming. *Nature Climate Change*, *3*, 563–566, https://doi.org/10.1038/nclimate1827

Ebi, K.L., Capon, A., Berry, P., et al. (2021). Hot weather and heat extremes: health risks. *The Lancet*, *398*, 698–708, https://doi.org/10.1016/S0140-6736(21)01208-3

Eyring, V., Bony, S., Meehl, G.A., et al. (2016). Overview of the coupled model intercomparison project phase 6 (cmip6) experimental design and organization. *Geoscientific Model Development*, *9*, 1937–1958, https://doi.org/10.5194/gmd-9-1937-2016

Foster, J., Smallcombe, J.W., Hodder, S., Jay, O., Flouris, A.D., Havenith, G. (2022). Quantifying the impact of heat on human physical work capacity; part ii: the observed interaction of air velocity with temperature, humidity, sweat rate, and clothing is not captured by most heat stress indices. *International Journal of Biometeorology*, *66*(3), 507–520, https://doi.org/10.1007/s00484-021-02212-y

Foster, J., Smallcombe, J.W., Hodder, S., Jay, O., Flouris, A.D., Nybo, L., Havenith, G. (2022). Quantifying the impact of heat on human physical work capacity; part iii: the impact of solar radiation varies with air temperature, humidity, and clothing coverage. *International Journal of Biometeorology*, *66*(1), 175–188, https://doi.org/10.1007/s00484-021-02205-x

Foster, J., Smallcombe, J.W., Hodder, S., et al. (2021). An advanced empirical model for quantifying the impact of heat and climate change on human physical work capacity. *International Journal of Biometeorology*, *65*(7), 1215–1229, https://doi.org/10.1007/s00484-021-02105-0

Hersbach, H., Bell, B., Berrisford, P., et al. (2020). The era5 global reanalysis. *Quarterly Journal of the Royal Meteorological Society*, *146*, 1999–2049, https://doi.org/10.1002/qj.3803

ISO (2017). *Ergonomics of the thermal environment – assessment of heat stress using the wbgt index* (Tech. Rep. No. ISO 7243:2017). Geneva, Switzerland: International Organization for Standardization.

Kjellstrom, T., Holmer, I., Lemke, B. (2009). Workplace heat stress, health and productivity–an increasing challenge for low and middle-income countries during climate change. *Global Health Action*, *2*, 2047, https://doi.org/10.3402/gha.v2i0.2047

Kong, Q., & Huber, M. (2022). Explicit calculations of wet-bulb globe temperature compared with approximations and why it matters for labor productivity. *Earth's Future*, *10*(3), e2021EF002334, https://doi.org/10.1029/2021EF002334

Li, D., Yuan, J., Kopp, R.E. (2020). Escalating global exposure to compound heat-humidity extremes with warming. *Environmental Research Letters*, *15*(6), 064003, https://doi.org/10.1088/1748-9326/ab7d04

Matthews, T.K.R., Wilby, R.L., Murphy, C. (2017). Communicating the deadly consequences of global warming for human heat stress. *Proceedings of the National Academy of Sciences of the United States of America*, *114*(15), 3861–3866, https://doi.org/10.1073/pnas.1617526114

Mora, C., Dousset, B., Caldwell, I.R., et al. (2017). Global risk of deadly heat. *Nature Climate Change*, *7*, 501–506, https://doi.org/10.1038/nclimate3322

O'Neill, B.C., Kriegler, E., Riahi, K., et al. (2014). A new scenario framework for climate change research: the concept of shared socioeconomic pathways. *Climatic Change*, *122*, 387–400, https://doi.org/10.1007/s10584-013-0905-2

O'Neill, B.C., Tebaldi, C., van Vuuren, D.P., Eyring, V., Friedlingstein, P., et al. (2016). The scenario model intercomparison project (ScenarioMIP) for CMIP6. *Geoscientific Model Development*, *9*, 3461–3482, https://doi.org/10.5194/gmd-9-3461-2016

Parsons, K. (2006). *Human thermal environments: The effects of hot, moderate, and cold environments on human health, comfort and performance.* Boca Raton: CRC Press.

Perkins, S.E., & Alexander, L.V. (2013). On the measurement of heat waves. *Journal of Climate*, *26*(13), 4500 - 4517, https://doi.org/10.1175/JCLI-D-12-00383.1

Raymond, C., Matthews, T., Horton, R.M. (2020). The emergence of heat and humidity too severe for human tolerance. *Science Advances*, *6*(19), eaaw1838, https://doi.org/10.1126/sciadv.aaw1838

Rothfusz, L.P. (1990). *The heat index equation (or, more than you ever wanted to know about heat index)* (Tech. Rep. No. SR 90-23). Fort Worth, TX: National Weather Service.

Sahu, S., Sett, M., Kjellstrom, T. (2013). Heat exposure, cardiovascular stress and work productivity in rice harvesters in india: implications for a climate change future. *Industrial Health*, *51*(4), 424–431, https://doi.org/10.2486/indhealth.2013-0006

Sherwood, S.C., & Huber, M. (2010). An adaptability limit to climate change due to heat stress. *Proceedings of the National Academy of Sciences*, *107*(21), 9552–9555, https://doi.org/10.1073/pnas.0913352107

Simpson, C., Hosking, J.S., Mitchell, D., Betts, R.A., Shuckburgh, E. (2021). Regional disparities and seasonal differences in climate risk to rice labour. *Environmental Research Letters*, *16*(12), 124004, https://doi.org/10.1088/1748-9326/ac3288

Stull, R. (2011). Wet-bulb temperature from relative humidity and air temperature. *Journal of Applied Meteorology and Climatology*, *50*(11), 2267–2269, https://doi.org/10.1175/JAMC-D-11-0143.1

Thrasher, B., Wang, W., Michaelis, A., Melton, F., Lee, T., Nemani, R. (2022). Nasa global daily downscaled projections, cmip6. *Scientific Data*, *9*(1), 262, https://doi.org/10.1038/s41597-022-01393-4 Retrieved from https://doi.org/10.1038/s41597-022-01393-4

Vanos, J., Guzman-Echavarria, G., Baldwin, J.W., et al. (2023). A physiological approach for assessing human survivability and liveability to heat in a changing climate. *Nature Communications*, *14*, 7653, https://doi.org/10.1038/s41467-023-43121-5

Vecellio, D.J., Wolf, S.T., Cottle, R.M., Kenney, W.L. (2022). Evaluating the 35°c wet-bulb temperature adaptability threshold for young, healthy subjects. *Journal of Applied Physiology*, *132*(2), 340–345, https://doi.org/10.1152/japplphysiol.00738.2021

Wang, X., Meng, X., Long, Y. (2022). Projecting 1 km-grid population distributions from 2020 to 2100 globally under shared socioeconomic pathways. *Scientific Data*, *9*, 563, https://doi.org/10.1038/s41597-022-01675-x

Zhao, Z., Yin, S., Hall, J. (2025). Can wet heatwaves be represented by cmip6 models and bias-corrected nex-gddp-cmip6? *Weather and Climate Extremes*, *50*, 100790, https://doi.org/10.1016/j.wace.2025.100790